JOURNAL OF PROPULSION AND POWER
Vol. 10, No. 2, March–April 1994

Anode Power Deposition in an Applied-Field Segmented Anode MPD Thruster

A. D. Gallimore*
Princeton University, Princeton, New Jersey 08544
R. M. Myers†
Sverdrup Technology, Inc., Brook Park, Ohio 44135
and
A. J. Kelly‡ and R. G. Jahn§
Princeton University, Princeton, New Jersey 08544

Anode heat flux measurements of a water-cooled segmented anode applied-field MPD thruster were made to investigate anode heat transfer phenomena. Pure argon and argon-hydrogen mixtures were used as propellants for a variety of thruster currents, propellant mass flow rates, and axial applied magnetic field strengths. The thruster was operated in two modes: 1) with all four segments active, and 2) with two of the segments floating. The results of this work show that the heat flux to the anode increases monotonically with axial magnetic field strength and thruster current. Between 50–75% of the anode heat flux is transported by the current-carrying electrons. Convective and radiative heat transfer (primarily from the cathode radiation) account for the remaining portion of the power deposited to the anode. The addition of hydrogen to the argon propellant results in the reduction of the fraction of anode power deposited by the anode fall to a level equivalent to that of convection and radiation.

Nomenclature

e = elementary charge, 1.6×10^{-19} C
J = anode segment current, A
Jt = total anode current, A
ja = anode current density, A/cm^2
k = Boltzmann's constant, 1.38×10^{-23} J/K
P = anode segment power, W
P_t = total anode power, W
$\dot{q}a$ = anode heat flux, W/cm^2
$\dot{q}c$ = anode heat flux from convection, W/cm^2
$\dot{q}r$ = anode heat flux from radiation, W/cm^2
Te = electron temperature, K
Ua = characteristic anode voltage, V
Va = anode fall, V
ϕ = anode material work function, 4.62 V

Introduction

ANODE power deposition has long been recognized as a major loss mechanism for MPD thrusters. For thrusters operating at power levels of 250 kW or less, most of the input power is wasted in heating the anode. Therefore, anode losses must be reduced if MPD thrusters are to become competitive with chemical or nuclear thermal rockets for near-term applications to spacecraft propulsion.[1,2] Given the complexity of the interaction of the anode with the adjacent plasma and our poor understanding of anode processes, researchers are forced to use experimental studies for insight.

Numerous anode heat-transfer studies have been made using a variety of electrode geometries and plasmas in seeded MHD generators and accelerators,[3–6] free "burning" arcs,[7,8] as well as MPD thrusters.[9–19] The goals of much of these studies were 1) to establish a data base of anode phenomena, 2) to search for trends in anode processes, and 3) to assist in the design and verification of anode models. One approach frequently taken in MPD thruster anode research has been to divide the anode into independent segments whereby current and heat flux distributions can be obtained.[10,11,15–18] Much of this work has been applied primarily to two types of steady-state thrusters, low-power (~20 kW) MPD thrusters with strong axial applied magnetic fields (>1000 G) and propellant flow rates of approximately 20 mg/s,[9–12] and high-power (>100 kW) self-field MPD thrusters with propellant flow rates on the order of 1 g/s.[16–18] There is, however, little information on anode power deposition in 100-kW class applied-field MPD thrusters with propellant flow rates of approximately 0.1 g/s. Given the promising results of recent work,[19] which shows that thruster performance can be enhanced through use of applied magnetic fields, there is renewed interest in using 100-kW class applied-field MPD thrusters for applications ranging from payload orbit raising to unmanned planetary missions.[2]

The primary goal of this research is to investigate the influence of thruster operating characteristics such as propellant selection, propellant flow rate, current, and applied magnetic field strength on anode power deposition in a 100-kW class MPD thruster. The segmented anode thruster uses argon and argon-hydrogen mixtures as propellant with mass flow rates between 50–150 mg/s. The thruster is operated at currents of 750–1250 A with axial applied magnetic field strengths [measured at the cathode tip (based on computer models, the axial magnetic field strength at the anode face is expected to be within 20% of the field strengths measured at the cathode tip)] between 300–800 G. The anode of the thruster is composed of four water-cooled copper segments. Current and heat flux to each segment are independently measured. Lang-

Presented as Paper 91-2343 at the AIAA/SAE/ASME 27th Joint Propulsion Conference, Sacramento, CA, June 24–27, 1991; received Sept. 21, 1991; revision received July 1, 1993; accepted for publication July 7, 1993.

*Graduate Assistant, Department of Mechanical and Aerospace Engineering; currently Assistant Professor, Department of Aerospace Engineering, University of Michigan, Ann Arbor, MI 48109. Member AIAA.

†Plasma Propulsion Engineer, NASA Lewis Research Center. Member AIAA.

‡Manager and Senior Research Engineer, Electric Propulsion Laboratory. Member AIAA.

§Professor, Department of Mechanical and Aerospace Engineering. Fellow AIAA.

muir probes are employed in the plume to measure electron temperatures which, with segment current and heat flux, permit an estimate of the local anode fall to be made.

Experimental Apparatus

The vacuum facility at the NASA Lewis Research Center used for these experiments consists of a test section, 3 m in diameter and 3-m long, that is attached to a 7.6-m-diam, 21-m-long vacuum chamber through a 3-m gate valve. Nineteen 81-cm-diam hydrocarbon oil diffusion pumps, backed by three Roots blowers and two mechanical pumps, maintain tank pressure to below 0.07 Pa (5×10^{-4} Torr) during thruster operation (~0.15 g/s argon). This pressure is below that known to affect the operation of applied-field MPD thrusters.[20] Facility pressure is monitored at four locations: 1) on the thrust stand, 2) along the chamber wall of the 3-m test section, and in the main chamber, 3) 12-, and 4) 16-m downstream of the thruster.

Thruster power is supplied by a series-parallel network of commercial arc welding power supplies providing a maximum output of 3000 A at 130 V (390 kW). Power to the electromagnet is provided by an additional arc welding power supply capable of delivering up to 1500 A at 44 V. Power to the thruster and magnet is transferred through water-cooled flexible copper cables.

Distilled and de-ionized cooling water for the thruster and magnet are provided by two closed-loop pump/heat exchanger assemblies each capable of supplying up to 0.8 l/s of water at pressures up to 1 MPa. Water flow rates are monitored with calibrated turbine flow sensors capable of measuring flow rates accurately to within 3%. Additional descriptions of the test facility can be found in Refs. 21 and 22.

MPD Thruster Assembly

A schematic diagram of the MPD thruster assembly used for this work is shown in Fig. 1. The assembly contains the thruster, magnet (not shown), current and water cooling lines, current sensors, water flow sensors, thermocouples, and assorted sensor signal and power lines (not shown). The entire assembly is placed on an inverted pendulum thrust stand designed to accommodate 250-kW class MPD thrusters. The thrust stand is routinely calibrated before and after each run, resulting in thrust measurements accurate to within 2%. A large rectangular radiation shield made of stainless steel and tantalum protects the assembly from plume radiation.

The thruster used for this experiment (cf. Fig. 2) features an anode composed of four independent water-cooled segments. Electrical and thermal isolation of each segment is provided by mica inserts whose inner surfaces are recessed slightly for protection against the discharge. Each anode segment has an inner and outer diameter (o.d.) of 8.9 and 12.7

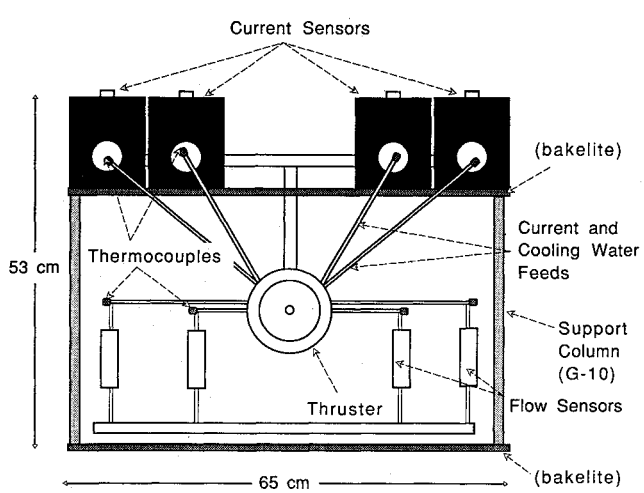

Fig. 1 MPD thruster assembly.

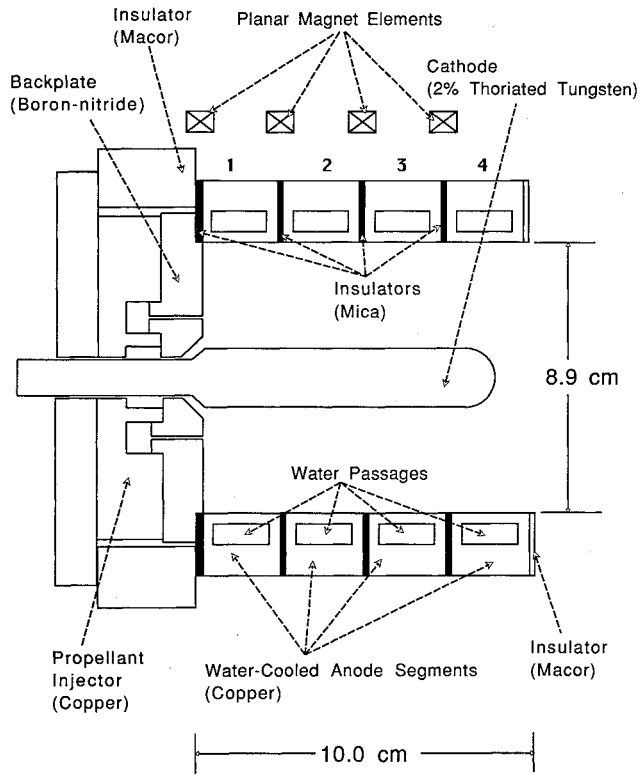

Fig. 2 Segmented anode MPD thruster.

cm, respectively, and is 2.2-cm long. The cooling water passage of each segment has a rectangular cross section measuring 1.6 by 0.6 cm with an anode wall thickness of 0.3 cm. Cooling water and current are provided to each segment through 1-cm-o.d. copper tubing. All active segments are connected to a common 2.5-cm-o.d. copper tube which also served as a plenum for the cooling water.

Mica insulation is also used to thermally insulate the first upstream segment (segment 1) from the boron-nitride back plate. The exposed face of the exit anode segment (segment 4) is insulated with macor to restrict current attachment to the interior of the thruster chamber, ensuring that all segments have equal electrode surface areas. The segments are held together with eight axial stainless steel threaded rods which traverse through the segments and insulators 5.9-cm radially from the thruster centerline.

Propellant is injected through the backplate by way of 24 1.6-mm-diam holes at a radius of 1.9 cm, and through an annulus around the base of the cathode. An equal amount of propellant flows through the holes and through the annulus. The cathode, constructed out of 2% thoriated tungsten, is 7.6 cm long and 1.8 cm in diameter, and is held in place by a water-cooled copper clamp located behind the propellant injector. Cooling water is passed through the cathode clamp prior to distribution to the anode segments. Water throughput for the entire thruster is approximately 0.4 l/s.

The electromagnet consists of four planar elements each with an inner diameter (i.d.) of 14 cm and an o.d. of 25 cm. Each element contains five turns of 1-cm-o.d. copper tubing providing passage for water flow rates of up to 0.3 l/s. Each magnet element is aligned with a mica insulator. The magnet is designed to provide an axial magnetic field strength of up to 1000 G at the cathode tip for magnet currents up to 1200 A. A computer code is employed to predict the shape and magnitude of the static field (with no discharge current) generated by this magnet. The predicted field profiles are similar to those produced by a solenoid of equivalent dimensions. A Hall probe is used to make static magnetic field measurements throughout the thruster. Calculated and measured field

strengths at various locations within the thruster compare quite favorably.

Cooling water flow rates for each segment are monitored with Omega FP-541 flow sensors which provide measurements accurate to within 1% (full scale). These plastic flow meters are also used to electrically isolate the anode and cathode current/cooling water supply lines from each other. Water temperature is measured with type K thermocouples enclosed in 0.3-cm-o.d. stainless steel sheaths that are concentric with the water passages. Cooling water temperature is monitored at the cathode clamp as well as at the magnet. Current to each segment is measured with F.W. Bell IF-5020P current sensors to within 1% accuracy. Segment voltages with respect to the cathode are measured with isolation amplifiers that are accurate to within ± 0.5 V.

In addition to calorimetric measurements of anode power deposition, electron temperature and ion density profiles in the plume are obtained as well. A description of the Langmuir probe system and methods used for data reduction are presented in Ref. 23. Acquisition of all data and thruster operating parameters is performed by a Keithley System 500 data-acquisition system driven by a Compaq personal computer.

Results

Figure 3 shows the distribution of current to the segments at three thruster currents and two applied field strengths, where J/Jt is the fraction of thruster current that is carried by a segment. At these operating conditions, 60–75% of the total input power is deposited into the anode. As the figure shows, most of the current is concentrated at the upstream- and downstream-most segments (1 and 4, respectively). The uneven segment current distribution shown is characteristic of "bimodal" axial current profiles seen in quasisteady (self-field) MPD thrusters of similar geometries.[24,25] This result is similar to that observed by Baksht et al.[26] and Schall[27] in which the intersection of magnetic field lines with the anode greatly enhanced current conduction. At the middle segments (2 and 3), the magnetic field lines are parallel with the anode impeding current conduction. At the end segments (1 and 4) however, the magnetic field lines intersect the anode, allowing current to reach these segments more easily.

The heat flux to the anode of a MPD thruster may be described by the following equation[28]:

$$\dot{q}a = ja[Va + \tfrac{5}{2}(kTe/e) + \phi] + \dot{q}c + \dot{q}r \qquad (1)$$

This equation represents the contribution to anode heating from the kinetic energy that current-carrying electrons gain from the potential difference between the anode and the local plasma, known as Va, the random electron thermal energy $[\frac{5}{2}(kTe/e)]$, the heat liberated due to ϕ, and contributions from plasma $\dot{q}c$ and $\dot{q}r$. The contribution to anode heating from convection and radiation, while negligible for high-power, quasisteady MPD thrusters which operate with cold cathodes and which have associated anode heat fluxes of several kilowatts per square centimeter,[13,14,29] may be important for 100-kW class steady-state thrusters with significantly lower levels of anode heat flux. This fact is illustrated in Fig. 4 where P/Pt represents the measured fraction of anode power that is absorbed by each individual segment. The figure shows that a significant function of the power deposited to the anode (Pt) is absorbed by anode segments 2 and 3, which do not receive a substantial amount of the arc current. Therefore, the bulk of power that is deposited to these segments is due to convection and radiation.

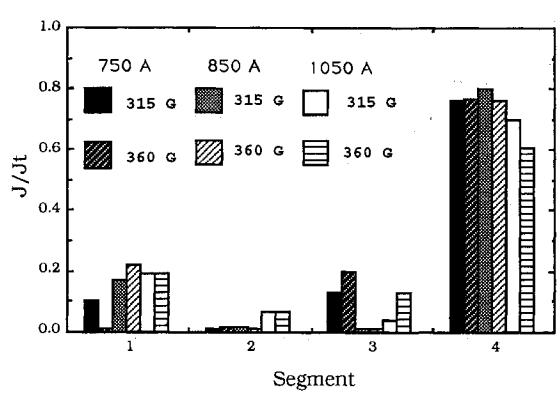

Fig. 3 Segment current distribution (100 mg/s argon).

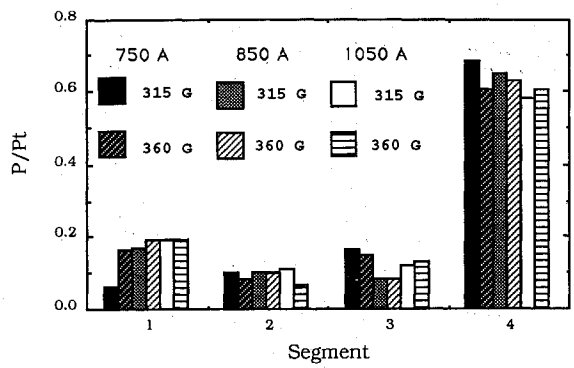

Fig. 4 Segment heat flux distribution (100 mg/s argon).

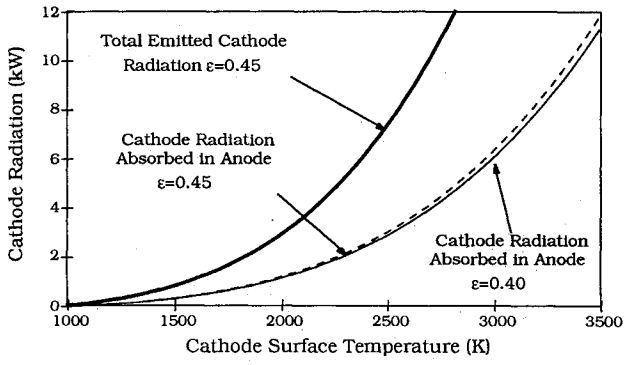

Fig. 5 Power of cathode radiation absorbed by anode.

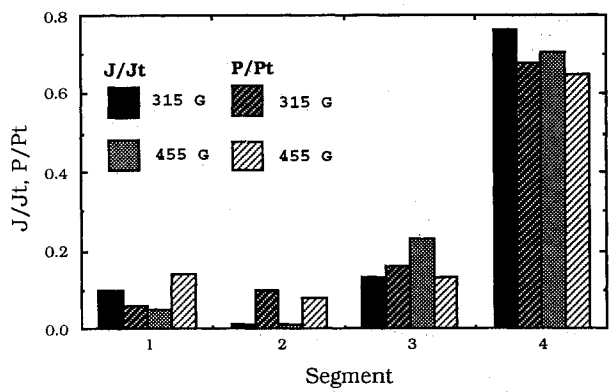

Fig. 6 Segment current and heat flux distribution (750 A, 100 mg/s argon).

It is estimated that for a cathode surface temperature between 3000–3200 K, up to 8 kW of cathode radiation is absorbed at the anode (cf. Fig. 5).[30] This corresponds roughly to between 10–25% of the total power deposited to the anode of a thruster operating at 100 kW. Under most operating conditions, the amount of power absorbed at the anode of MPD thrusters from plasma radiation is negligible. Therefore, the radiation term in Eq. (1) will primarily consist of cathode radiation.

Figure 6 shows anode current and heat flux distributions as a function of applied field strength. An increase in field strength results in more current flow to the two downstream segments. In agreement with Eq. (1), it is also seen that the amount of

heat absorbed at each segment is greatly influenced by the current. Although segment 2 receives only 1 or 2% of the current, it still accounts for 10% of the anode power. This further illustrates that convection and cathode radiation, although negligible for pulsed devices, may not be neglected in steady-state devices.

The results presented thus far suggest that for any operational steady-state MPD thruster, a non-negligible fraction of the anode power will have as its source convection and cathode radiation. Therefore, these important modes of anode power deposition cannot be ignored in anode fall estimates for steady-state thrusters which rely on anode heat flux data. For this reason, a series of tests was performed where segments 1 and 2 (cf. Fig. 2) were electrically isolated from the power supply to serve as a means of measuring anode power deposition due to convection and cathode radiation.

Current and heat flux distributions for the reconfigured thruster are shown in Fig. 7. As the figure shows, the current and heat flux pattern has become less concentrated with increased field strength, a trend that was observed throughout the experimental program. It is also seen that the two floating segments each consume between 5–10% of the anode power, the same amount as that absorbed by the segment (2) that carried little current in the case in which all four segments were active (cf. Fig. 6). This implies that one is justified in using the heat flux to a floating electrode for the estimate of anode heating from convection and radiation.

Allowing thruster current to flow to the two downstream segments only results in higher terminal voltages which almost all appears as increased anode voltage. This effect can be seen in Fig. 8 which shows the terminal voltage and the *Ua*, defined as the total power consumed by the anode divided by the total current, as a function of applied field strength. Because of these higher operating voltages, the thruster with four active segments has slightly better performance than the reconfigured device. Although observed in other segmented anode studies,[10] an explanation for this observation cannot be given at this time.

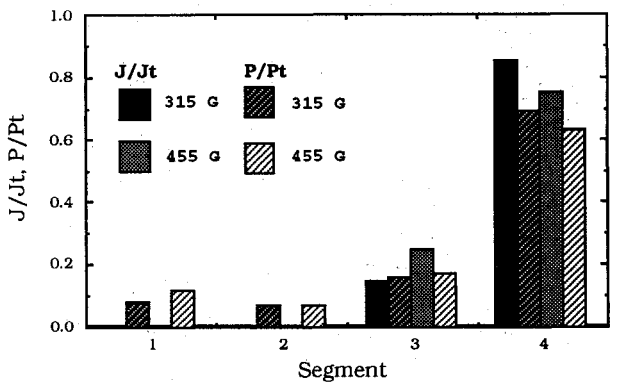

Fig. 7 Segment current and heat flux distribution (2 active segments; 750 A, 100 mg/s argon).

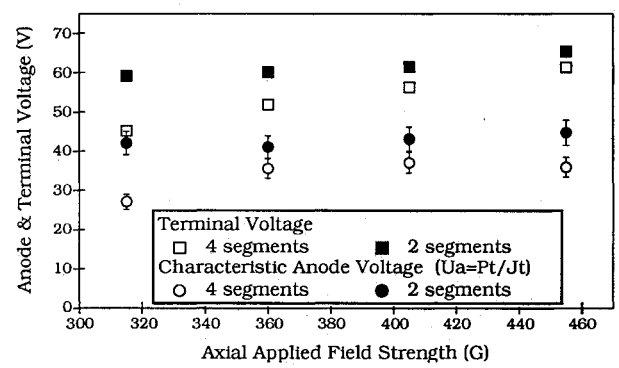

Fig. 8 Characteristic anode voltage and terminal voltage vs applied field strength (750 A, 100 mg/s argon).

Figures 9 and 10 show how power deposited to the floating segments through convection and radiation varies with applied field strength, thruster current, and hydrogen propellant fraction. As seen in Fig. 9a, power to the floating segments increases linearly with applied field strength. Through filtered photographic techniques, the cathode has been observed to become hotter with increasing magnetic field strength. Thus, a large part of this two-fold increase in segment power is likely caused by an increase in emitted cathode radiation.

As shown in Fig. 9b, above 850 A heat flux to the segments increases linearly with current, a trend which is also consistent with an increase in cathode temperature. As the current increases, the difference between the power absorbed at segments 1 and 2 also becomes larger. The effect of adding hydrogen to the argon propellant on convective and radiative anode heat transfer is presented in Fig. 10. Floating segment power remains constant for hydrogen propellant mass fractions up to 5%. Beyond this, there is a large increase in segment power and a large variation in power between segments 1 and 2. At a hydrogen mass fraction of 30%, 6–9 kW of power is deposited at each segment by convection and radiation. This magnitude of power is too much to be accounted for by cathode radiation alone (cf. Fig. 5).

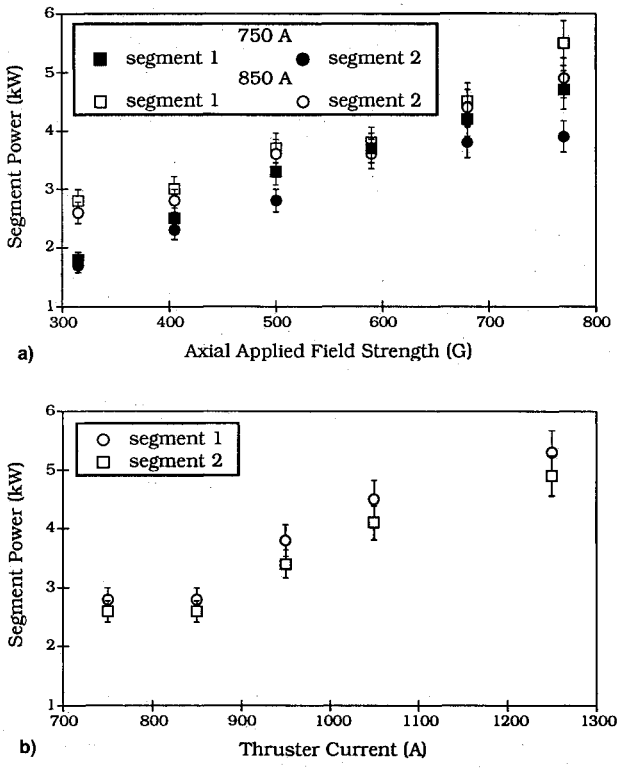

Fig. 9 Power deposition to floating segments: a) 140 mg/s argon and 3 mg/s hydrogen and b) 100 mg/s argon and hydrogen.

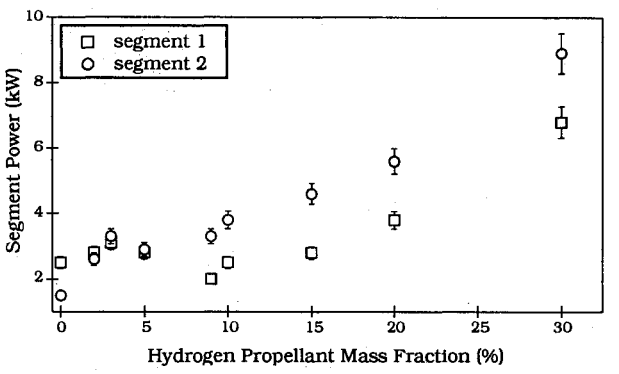

Fig. 10 Power deposition to floating segments (850 A, 315 G).

Estimated Anode Falls

The anode fall plays a dominant role in the deposition of power to the anode. In order to fully understand anode power dissipation, the dependence of the anode fall on field strength, propellant selection, and thruster current must be established. By manipulating the equation for energy balance at the anode [Eq. (1)] we obtain the following relation for the anode fall:

$$Va = \frac{\dot{q}a - \dot{q}c - \dot{q}r}{ja} - \left[\frac{5}{2}\left(\frac{kTe}{e}\right) + \phi\right] \qquad (2)$$

To calculate Va, the following assumptions were made:

1) Heat flux contributions from convection and radiation ($\dot{q}c + \dot{q}r$) to each current-carrying segment were assumed to be the mean of the fluxes measured at segments 1 and 2.

2) An electron temperature of 1.3 eV (15,000 K) was used for all calculations. This value was obtained from extrapolation of electron temperatures measured in the plume by Langmuir probes.[23,31,32]

Figure 11 shows the dependence of the anode fall and anode heat transfer modes on applied field strength for an argon-hydrogen mixture. Two means were used to calculate the anode falls: 1) use of Eq. (2) with all the accompanying assumptions mentioned above (labeled calorimetric in figures); and 2) employment of segment 3 as a floating probe (labeled as potential in figures). The measured floating potential was corrected to plasma potential by using an electron temperature of 1.3 eV. As is illustrated in Fig. 11a, the estimated anode falls of the two active segments are quite different. The anode fall for segment 3 remains constant, while that of segment 4, as determined through calorimetry, increases with field strength.

This difference becomes more pronounced at large values of applied field strength. Good agreement between the "calorimetric" and "potential" estimates of the anode fall exists only for segment 3 at applied field strengths below 600 G, implying that both axial and radial electric fields present near the anode are sensitive to the magnetic field strength. Strong axial gradients have been observed in quasisteady devices of similar geometry.[33,34]

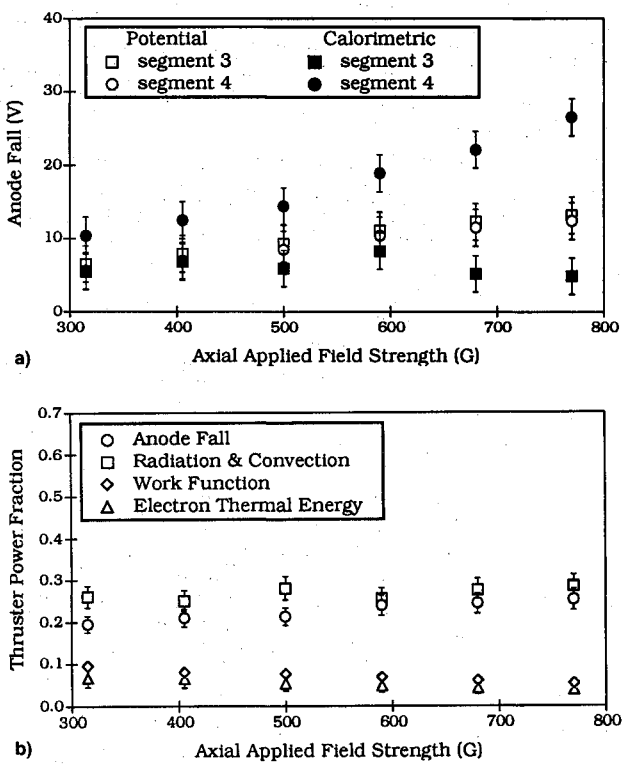

Fig. 11 a) Anode fall and b) anode power fraction components vs applied field strength (850 A, 140 mg/s argon and 3 mg/s hydrogen).

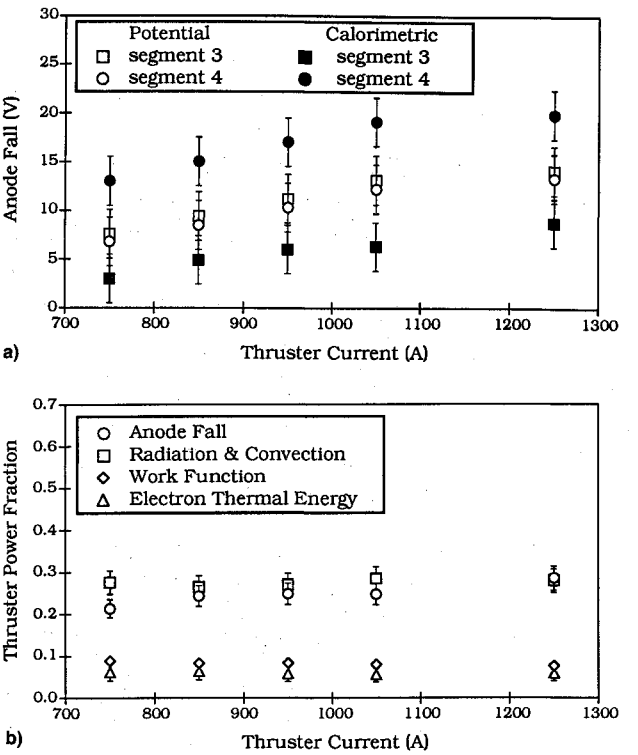

Fig. 12 a) Anode fall and b) anode power fraction components vs thruster current (315 G, 100 mg/s argon and 3 mg/s hydrogen).

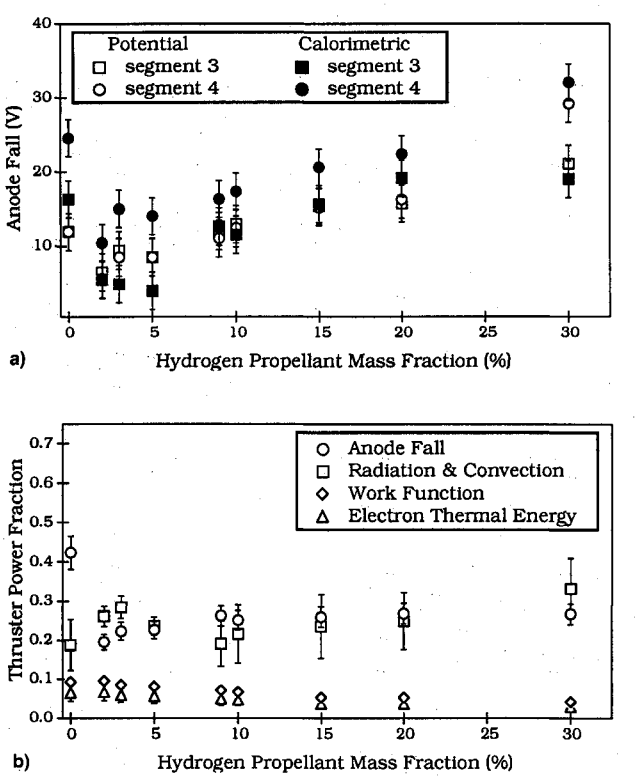

Fig. 13 a) Anode fall and b) anode power fraction components vs hydrogen propellant mass fraction (850 A, 315 G).

With the exception of the calorimetric measurements of segment 4, both the anode fall and the thruster power fraction consumed by it are seen not to increase rapidly with applied field strength for these operating conditions (cf. Fig. 11b). Of special note is the fact that the contribution to anode heating from the anode fall is actually slightly less than that due to convection and radiation.

Figure 12 shows the dependence of the anode fall and anode power modes on thruster current for a mixture of argon and hydrogen propellants. As shown by Fig. 12a, below a current of 1050 A the anode fall in both segments increases with current. Anode fall estimates based on floating segment potential measurements are between the calorimetrically determined values for segments 3 and 4. Figure 12b shows that once again contributions from radiation and convection are on par with those from the anode fall, all of which accounts for over 40% of the thruster power.

Figure 13 shows the variation of the anode fall and anode power fraction components with mass fraction of argon and hydrogen propellants. Initially, the addition of hydrogen greatly reduces the anode fall of both active segments. Beyond 5% hydrogen propellant fraction however, the introduction of more hydrogen results in increased anode falls of both segments. In addition, the difference between calorimetrically determined anode fall estimates and those measured by the floating segment decreases with increasing hydrogen propellant fraction. Between hydrogen propellant fractions of 5–30%, the difference in the anode falls of segments 3 and 4 is less than 5 V. The behavior of the anode fall depicted in Fig. 13a closely resembles that of the power input to the floating segments (cf. Fig. 10). Furthermore, in Fig. 13b it is seen that the addition of hydrogen reduces the contribution of the anode fall to anode power deposition to a level equivalent to that of convection and radiation.

Conclusions

Experimental results with an applied-field segmented-anode MPD thruster show that the magnitude of power deposition to the anode increases with increasing field strength. This increase is manifested in the anode fall as well as in convective and radiative heat transfer modes. In addition, for the operating conditions studied, the applied-field strength is not found to have a major impact on anode power fraction. This conclusion, however, is tempered somewhat by results obtained by Myers,[35] who found that over a much larger range of applied-field strengths (0–2000 G), anode power fraction decreases with increasing applied-field strength. Results from our experiments show thruster current to have slightly less impact on anode power deposition than the applied field. The addition of hydrogen propellant to the argon has the most significant effect on anode power deposition, resulting in a reduction in the anode fall power fraction. The addition of hydrogen also results in increased anode power deposition from convection and radiation. An optimum range of hydrogen propellant fraction appears to be between 1–10%. Finally, heat transfer measurements to floating segments show that convection and radiation contribute a substantial fraction of the power that is deposited to the anode for 100-kW class steady-state MPD thrusters. Radiation emanating from the cathode is shown to be an important contribution to anode heating for 100-kW class steady-state MPD thrusters.

Acknowledgments

This research was supported by a grant from the NASA Minority Graduate Program, a component of the NASA Graduate Student Researchers Program, and in part by NASA Grant Contract 954997. The authors wish to thank Mike LaPointe for the use of his computer code (BCOILS.FOR) in the calculation of electromagnetic field profiles, and Larry Schultz, David Wolford, Olin Reed, John Miller, John Eckert, Gerry Schneider, John McAlea, Robert Butler, and Tom Ralys for their assistance at the NASA Lewis Research Center.

References

[1]Palaszewski, B., "Electric Propulsion Parameters for Manned Mars Exploration," 1989 JANNAF Propulsion Meeting, Chemical Propulsion Information Agency, Laurel, MD, May 1989.

[2]Hack, K. J., George, J. A., Riehl, J. P., and Gilland, J. H., "Evolutionary Use of Nuclear Electric Propulsion," AIAA Paper 90-3821, Sept. 1990.

[3]Kerrebrock, J. L., "Electrode Boundary Layers in Direct-Current Plasma Accelerators," *Journal of Aerospace Sciences*, Vol. 3, No. 8, 1961, pp. 631–643.

[4]High, M. D., and Felderman, E. J., "Turbulent MHD Boundary Layers with Electron Thermal Non-Equilibrium and Finite Rate Ionization," *AIAA Journal*, Vol. 10, No. 1, 1972, pp. 98–103.

[5]Karkosak, J. J., and Hoffman, M. A., "Electrode Drops and Current Distribution in an MGD Channel," *AIAA Journal*, Vol. 3, No. 6, 1965, pp. 1198–1200.

[6]Kent, J. R., and Kruger, C. H., "Joule Heating Effects in MHD Generators Boundary Layers," *AIAA Journal*, Vol. 21, No. 5, 1983, pp. 679–686.

[7]Merinov, N. S., Ostretsov, I. N., Petrosov, V. A., and Porotnikov, A. A., "Anode Processes with a Negative Potential Drop at the Anode," *Soviet Physics Technical Physics*, Vol. 21, No. 4, 1983, pp. 467–472.

[8]Sanders, N. A., and Pfender, E., "Measurements of Anode Falls and Anode Heat Transfer in Atmospheric Pressure High Intensity Arcs," *Journal of Applied Physics*, Vol. 55, No. 3, 1984, pp. 714–722.

[9]Shih, K. T., Pfender, E., Ibele, W. E., and Eckert, E. R. G., "Experimental Anode Heat-Transfer Studies in a Coaxial Arc Configuration," *AIAA Journal*, Vol. 6, No. 8, 1968, pp. 1482–1487.

[10]Shih, K. T., "Anode Current and Heat Flux Distributions in an MPD Engine," AIAA Paper 69-244, March 1969.

[11]Bose, T. K., and Pfender, E., "Direct and Indirect Measurements of the Anode Fall in a Coaxial Arc Configuration," *AIAA Journal*, Vol. 7, No. 8, 1969, pp. 1643–1645.

[12]Shih, K. T., and Pfender, E., "Electrode Energy Transfer Mechanisms in a MPD Arc," *AIAA Journal*, Vol. 8, No. 2, 1970, pp. 211–215.

[13]Saber, A. J., "Anode Power in a Quasi-Steady MPD Thruster," Dept. of Aerospace and Mechanical Sciences, Princeton Univ., Princeton, NJ, 1974.

[14]Oberth, R. C., "Anode Phenomenon in High-Current Discharges," Ph.D. Dissertation, Dept. of Aerospace and Mechanical Sciences, Princeton Univ., Princeton, NJ, 1970.

[15]Hügel, H., "Effect of Self-Magnetic Forces on the Anode Mechanism of a High Current Discharge," *IEEE Transactions on Plasma Science*, Vol. PS-8, No. 4, 1980, pp. 437–442.

[16]Auweter-Kurtz, M., Kurtz, H. L., Merke, W. D., Scharde, H. O., and Christian Sleziona, P., "Self Field MPD Thruster Investigation," FY'88 Final Rept. (unpublished), Institute für Raumfahrtsysteme, Universität Stuttgart, IRS-88-P-10, Stuttgart, Germany.

[17]Auweter-Kurtz, M., Kurtz, H. L., Merke, W. D., Scharde, H. O., Christian Sleziona, P., and Wegmann, T., "High Power Steady State MPD Thruster," FY'89 Final Rept. (unpublished), Institute für Raumfahrtsysteme, Universität Stuttgart, IRS-90-P4, Stuttgart, Germany.

[18]Kurtz, H. L., Auweter-Kurtz, M., Merke, W. D., and Scharde, H. O., "Experimental MPD Thruster Investigations," AIAA Paper 87-1019, May 1987.

[19]Myers, R. M., Mantenieks, M. A., and Sovey, J. S., "Geometric Effects in Applied-Field MPD Thrusters," AIAA Paper 90-2669, July 1990.

[20]Sovey, J. S., and Mantenieks, M. M., "Performance and Lifetime Assessment of Magnetoplasmadynamic Arc Thruster Technology," *Journal of Propulsion and Power*, Vol. 7, No. 1, 1991, pp. 71–83.

[21]Sovey, J. S., Mantenieks, M. A., Haag, T. W., Raitano, P., and Parkes, J. E., "Test Facility and Preliminary Performance of a 100 kW Class MPD Thruster," 1989 JANNAF Propulsion Meeting, Cleveland, OH, May 1989.

[22]Haag, T. W., "Design of a Thrust Stand for High Power Electric Propulsion Devices," AIAA Paper 89-2829, July 1989; also NASA TM-102372, July 1989.

[23]Myers, R. M., Wherle, D., Vernyl, M., Biaglow, J., and Reese, S., "A Preliminary Characterization of Applied-Field MPD Thruster Plumes," AIAA Paper 91-2339, June 1991.

[24]Wolf, M. J., Kelly, A. J., and Jahn, R. G., "A High Performance Magnetoplasmadynamic Thruster," Japan Society for Aeronautical and Space Sciences, IEPC 84-32, Tokyo, April 1984, pp. 206–212.

[25]Heimerdinger, J. D., "Fluid Mechanics in a Magnetoplasmadynamic Thruster," Ph.D. Dissertation, Dept. of Aeronautics and Astronautics, Massachusetts Inst. of Technology, Cambridge, MA, 1988.

[26]Baksht, F. G., Moizhes, B. Ya., and Rybakov, A. B., "Critical Mode in a Coaxial Plasma Accelerator with External Magnetic Field," *Soviet Physics Technical Physics*, Vol. 21, No. 2, 1976, pp. 150–152.

[27]Schall, W., "Influence on Magnetic Fields on Anode Losses in MPD-Arcs," AIAA Paper 72-502, April 1972.

[28]Eckert, E. R. G., and Pfender, E., *Advances in Heat Transfer*, edited by J. P. Harnet and T. F. Irvine Jr., Vol. 2, Academic Press, NY, 1967, pp. 229–316.

[29]Gallimore, A. D., Kelly, A. J., and Jahn, R. G., "Anode Power Deposition in Quasi-Steady MPD Thrusters," AIAA Paper 90-2668, July 1990.

[30]Incropera, F. P., and DeWitt, D. P., *Fundamentals of Heat Transfer*, Wiley, New York, 1981.

[31]Myers, R. M., "Plume Characteristics of MPD Thrusters: A Preliminary Examination," AIAA Paper 89-2832, July 1989; also NASA CR-185130, July 1989.

[32]Gallimore, A. D., "Anode Power Deposition in Coaxial MPD Thrusters," Ph.D. Dissertation, Dept. of Mechanical and Aerospace Engineering, Princeton Univ., Princeton, NJ, 1992.

[33]Tahara, H., Kagaya, Y., and Yoshikawa, T., "Hybrid MPD Thruster with Axial and Cusp Magnetic Fields," IEPC 88-058, Oct. 1988, pp. 333–341.

[34]Kisov, A. Ya., Morozov, A. I., and Tilinin, G. N., "Distribution of Potential in a Quasistationary Coaxial Plasma Injector," *Soviet Physics Technical Physics*, Vol. 13, No. 6, 1968, pp. 467–472.

[35]Myers, R. M., "Applied-Field MPD Thruster Geometry Effects," AIAA Paper 91-2342, June 1991.